Creep Analysis Capability in MSC/NASTRAN

Sang Hoon Lee
Senior Project Engineer
The MacNeal-Schwendler Corporation

Synopsis

The creep analysis capability was introduced in MSC/NASTRAN Version 63. State-of-the-art theory and algorithms are employed to process the creep behavior coupled with the elastoplastic deformation at elevated temperatures. This formulation is based on the Maxwell-Kelvin rheological model. Various choices of empirical creep laws are available and small variations in temperature are allowed.

I. INTRODUCTION

At the macroscopic level, the creep phenomenon is best observed in the uniaxial creep test under constant load and the relaxation test under constant strain at constant temperature. A specimen subjected to a constant uniaxial tension at an elevated temperature exhibits three distinct phases in the time frame: primary creep stage, secondary creep stage and the tertiary creep stage to rupture as shown in Figure 1. If the specimen is unloaded after some creep deformation, the elastic strain is immediately recovered and a portion of the creep strain is gradually recovered as shown in Figure 2. The recoverable portion of the creep deformation is called primary creep and the non-recoverable portion is called secondary creep. The tertiary creep, similar to necking in plasticity, is considered as a localized instability phenomenon, which is beyond the scope of this creep analysis.

The Kelvin-Maxwell rheological model as developed in Reference [1] is employed in the formulation of the creep capability as a generalization of the viscoelastic material behavior. The step-by-step integration in time is performed assuming that the rheological model parameters remain constant for a short time interval (corresponding to a small change in stress). Several forms of empirical creep laws are available. When they are selected to characterize the creep behavior instead of direct input of rheological model

parameters, the program converts the empirical formula to the corresponding rheological model. This conversion is merely a mathematical exercise and is not shown in this paper for brevity. The rheological model parameters are functions of stress and temperature. The material routine adjusts the parameter values as the computation proceeds.

One of the virtues of the present method is the ability to accommodate stress reversal with ease. Effects of creep strain hardening can be properly reflected on the solution with stress reversal while no special provision is required.

The elastic-creep tangent modulus is formulated based on the Prandtl-Reuss stress-strain relationship. This tangent modulus is used for Newton's iteration to equilibrium at each time step. If the plastic deformation is coupled with creep, the material routine will seek a solution in two distinct steps. First, it solves for the incremental stress with an elastic-creep material. If the new stress state exceeds the current yield stress, a correction will be made on an incremental stress previously obtained and the plastic strain will be computed. The material routine will always return the elastic-creep material tangent for the formation of a global stiffness matrix.

II. USER INTERFACE

A nonlinear static analysis can readily be converted to creep analysis by adding a few creep related data cards. All the potentially nonlinear elements (RØD, BEAM, QUAD4, TRIA3, HEXA and PENTA) are applicable to creep analysis, but not all the nonlinear elements in the model must be made with creep material. All the other nonlinear data in the model, such as NLPARM (for iteration strategy), MATS1 (for plastic material) and PARAM, LGDISP (for geometric nonlinearity) are fully compatible with creep analysis.

The creep analysis is performed in SØL 66, using subcases following a subcase for static analysis. A flag for creep analysis is a positive value of Δt specified in the "DT" field of NLPARM card. Another subcase may be defined to change the value of Δt or the number of increments. The external load should remain constant (or change slowly if required) during the creep analysis. When the external (including thermal) loading on the structure changes, a new subcase should be defined for static analysis and subsequent subcases may be followed for creep analysis.

Creep characteristics are defined in the Bulk Data card CREEP. In the CREEP card, users are allowed to either specify an empirical creep law or provide direct input of rheological parameter values as functions of the effective stress using the TABLES1 card. If the creep behavior is prescribed by a creep law, creep law parameters will be converted to rheological parameters (K_p, C_p and C_s) whenever a new stress state is computed for the creep analysis. The empirical creep laws provided in MSC/NASTRAN are in the following equation forms:

$$\varepsilon^c(\sigma,t) = A(\sigma)\left[1 - e^{-R(\sigma)t}\right] + K(\sigma)t \qquad (1)$$

for all combinations of types 1 and 2 for A, R and K (types 111 through 222),

where A, R and K are expressed as

Parameter	Type 1	Type 2
$A(\sigma)$	$a\sigma^b$	a Exp $(b\sigma)$
$R(\sigma)$	c Exp $(d\sigma)$	$c\sigma^d$
$K(\sigma)$	$e[\sinh(f\sigma)]^g$	e Exp $(f\sigma)$

or $$\varepsilon^c(\sigma,t) = a\ \sigma^b t^d \qquad (2)$$

for type 300,

where a through b are user specified constants.

If the temperature distribution is different from the reference temperature specified on a CREEP card and if this effect needs to be analyzed, then the temperature distribution must be defined in the bulk data (TEMP, TEMPP1 or TEMPRB) and selected by a Case Control card (TEMP) in the subcase. In addition, a parameter card PARAM, TABS must be included to indicate the unit of temperature.

The numerical solution scheme employed in the creep analysis formulation is unconditionally stable. However, a limit should be placed on the time increment (Δt) to achieve a valid solution. The time increment should be selected so that the strain and/or stress do not change excessively in one increment. With excessive changes of strain or stress in a single step, the solution will deteriorate and errors will accumulate. Although the extent of excessiveness is problem-dependent, upper limits are set in the program using the stress and creep strain increment. The program will issue a warning message if this limit is exceeded.

III. EFFECTS OF CREEP STRAIN RATE

Microscopically, creep deformation is the integrated effect of dislocations of the crystal structure primarily due to thermal activation and stress. The effects of temperature at the microscopic level can be quantified as

$$\dot{\varepsilon}^{c} = A\, e^{-\Delta H/RT} \tag{3}$$

where ΔH is the energy of activation
R is the gas constant
T is the absolute temperature
A is in strain/unit time

An analytical solution to the Kelvin-Maxwell model (shown in Figure 3) subjected to constant stress (σ) is given as

$$\varepsilon^{c}_{total} = \frac{\sigma}{C_s} t + \varepsilon^{c}_{primary}$$

where

$$\varepsilon^{c}_{primary} = \frac{\sigma}{K_p}\left[1 - e^{-(K_p/C_p)t}\right] \tag{4}$$

For a varying stress problem, an instantaneous strain rate is required to have the creep hardening effect properly accounted. MSC/NASTRAN employs the strain hardening law by which creep strain rates are expressible in terms of creep strain rather than time. The strain hardening law of the rheological model is obtained upon differentiation of Eq. (4) and elimination of t, i.e.

$$\dot{\varepsilon}^{c}_{total} = \frac{\sigma}{C_s} + \dot{\varepsilon}^{c}_{primary}$$

where

$$\dot{\varepsilon}^{c}_{primary} = \frac{1}{C_p}\left(\sigma - K_p\, \varepsilon^{c}_{primary}\right) \tag{5}$$

In order to take into account strain hardening effects, $\varepsilon^{c}_{primary}$, corresponding to each stress component, is stored in memory. When the sign of the stress (σ) reverses, so does the sign of the creep strain rate with the strain hardening effect properly accounted for.

The creep strain rate is in general a function of the absolute temperature. Recalling Eq. (3), if the creep model parameters in Eq. (5) are determined based on the experimental data measured at the reference temperature (T_o), the creep strain rate can be corrected for the temperature, T, in the vicinity of T_o by applying a factor

$$F_c = \frac{\dot{\varepsilon}^c}{\dot{\varepsilon}^c_o} = \left(e^{-\Delta H/RTo}\right)^{\left(\frac{T_o}{T} - 1\right)} \tag{6}$$

The creep model parameters are corrected as

$$C_s(T) = \frac{C_s(T_o)}{F_c} \quad \text{and} \quad C_p(T) = \frac{C_p(T_o)}{F_c} \tag{7}$$

IV. EQUILIBRIUM CONDITION FOR A DEVIATORIC STRESS COMPONENT

Let us assume, for the time being, that the Maxwell-Kelvin rheological model is applied to a typical deviatoric stress component. The state equilibrium equation of the model at any instant can be expressed as:

$$[C]\ \{\dot{\Delta e}\} + [K]\ \{\Delta e\} = \{\Delta s\} \tag{8}$$

where

$$[C] = \begin{bmatrix} C_s & -C_s \\ -C_s & (C_p + C_s) \end{bmatrix}, \quad [K] = \begin{bmatrix} 0 & 0 \\ 0 & K_p \end{bmatrix}$$

and $\{\Delta s\}^T = \langle \Delta s_1 \quad 0 \rangle$ is the stress increment.

Using the central difference method, the strain rate increment may be expressed as

$$\dot{\Delta e} = \frac{2}{\Delta t}\left[\Delta e(t) - \dot{e}(t)\Delta t\right] .$$

Substitution of this equation into Eq. (8) results in

$$\left[\frac{2}{\Delta t} C + K\right]\ \{\Delta e\} = 2[C]\ \{\dot{e}\} + \{\Delta s\} . \tag{9}$$

Defining the stiffnesses of the primary and secondary creep elements by

$$\left.\begin{aligned} k_1 &= k_p + \frac{2C_p}{\Delta t} \\ k_2 &= \frac{2C_s}{\Delta t} \end{aligned}\right\} , \tag{10}$$

an equivalent creep stiffness can be determined by

$$k_c = \frac{k_1 k_2}{k_1 + k_2} \quad . \tag{11}$$

Then, solving Eq. (9) for Δe_1 gives

$$k_c \Delta e_1 = \Delta s' + \Delta s_1 \tag{12}$$

where $\Delta s'$ is a pseudo incremental stress, determined by

$$\Delta s' = 2\left[\frac{C_s}{k_2}(\dot{e}_1 - \dot{e}_2) + \frac{C_p}{k_1}\dot{e}_2\right]k_c \tag{13}$$

The pseudo incremental stress $\Delta s'$ represents the change in deviatoric stress component due to creep relaxation. This value of $\Delta s'$ can be converted to the equivalent psuedo incremental strain $\Delta e'$, which represents the change in deviatoric strain component due to creep. But by virtue of creep volume constancy $(\dot{\varepsilon}^c_x + \dot{\varepsilon}^c_y + \dot{\varepsilon}^c_z = 0)$, the deviatoric strains $(\Delta e')$ and the strain rates $(\dot{e}_1$ and $\dot{e}_2)$ in Eq. (13) are identical to the ordinary strain components. Hence $\Delta e'$ can be expressed as

$$\Delta \varepsilon' = \frac{\Delta s'}{k_c} = 2\left[\frac{C_s}{k_2}(\dot{\varepsilon}_1 - \dot{\varepsilon}_2) + \frac{C_p}{k_1}\dot{\varepsilon}_2\right] \tag{14}$$

in which the first term is a contribution of the secondary creep element $(\dot{\varepsilon}^c_{\text{secondary}})$ and the second term is a contribution of the primary creep element $(\dot{\varepsilon}^c_{\text{primary}})$. Notice that as Δt approaches zero, Eq. (14) reduces to

$$\Delta \varepsilon' \simeq \Delta t \dot{\varepsilon}_1 = \Delta t \dot{\varepsilon}^c_{\text{total}} \quad . \tag{15}$$

V. ADAPTATION OF RHEOLOGICAL MODEL TO MULTI-AXIAL STRESS STATE

The uniaxial creep behavior is extended to the general multiaxial stresses by introducing the concept of effective stress and effective strain as in plasticity. Adopting the Prandtl-Reuss stress-strain relationship, the creep strain-rates can be defined by

$$\{\dot{\varepsilon}^c\} = \frac{3}{2} \frac{\dot{\bar{\varepsilon}}^c}{\bar{\sigma}} \{S\} \tag{16}$$

where creep strain rates $\{\dot{\varepsilon}^c\}^T = < \dot{\varepsilon}_x^c \; \dot{\varepsilon}_y^c \; \dot{\varepsilon}_z^c \; \dot{\gamma}_{xy}^c \; \dot{\gamma}_{yz}^c \; \dot{\gamma}_{zx}^c >$,

deviatoric stresses $\{S\}^T = < \sigma_x' \; \sigma_y' \; \sigma_z' \; 2\tau_{xy} \; 2\tau_{yz} \; 2\tau_{zx} >$,

and the effective stress $(\bar{\sigma})$ and the effective creep strain rate $(\dot{\bar{\varepsilon}}^c)$ are defined as

$$\bar{\sigma} = \sqrt{\frac{1}{2}\left[(\sigma_x - \sigma_y)^2 + (\sigma_y - \sigma_z)^2 + (\sigma_z - \sigma_x)^2\right] + 3\left(\tau_{xy}^2 + \tau_{yz}^2 + \tau_{zx}^2\right)} \tag{17}$$

and $$\dot{\bar{\varepsilon}} = \frac{2}{3}\sqrt{\frac{1}{2}\left[(\dot{\varepsilon}_x - \dot{\varepsilon}_y)^2 + (\dot{\varepsilon}_y - \dot{\varepsilon}_z)^2 + (\dot{\varepsilon}_z - \dot{\varepsilon}_x)^2\right] + \frac{3}{4}\left(\dot{\gamma}_{xy}^2 + \dot{\gamma}_{yz}^2 + \dot{\gamma}_{zx}^2\right)}$$

Assumptions made in these constitutive relations are

i) the material is isotropic

ii) creep volume constancy: $\dot{\varepsilon}_x^c + \dot{\varepsilon}_y^c + \dot{\varepsilon}_z^c = 0$

iii) hydrostatic pressure cannot cause creep.

Implied by Eq. (16), there is a unique set of rheological parameters ($\bar{K}_p$, $\bar{C}_p$ and $\bar{C}_s$) based on the effective stress ($\bar{\sigma}$), which can be related to all the deviatoric stress components, i.e.

$$\frac{K_p}{\bar{K}_p} = \frac{C_p}{\bar{C}_p} = \frac{C_s}{\bar{C}_s} = \frac{2}{3} \text{ for } \sigma'_x \text{ , } \sigma'_y \text{, and } \sigma'_z$$

$$\frac{K_p}{\bar{K}_p} = \frac{C_p}{\bar{C}_p} = \frac{C_s}{\bar{C}_s} = \frac{1}{3} \text{ for } \tau_{xy}, \tau_{yz}, \text{ and } \tau_{zx} \tag{18}$$

Using Eq. (18), the stiffnesses of the creep model in Eq. (10) and the psuedo incremental strain in Eq. (14) may be rewritten in terms of effective creep model parameters, i.e.

$$\left.\begin{aligned} K_1 &= \frac{2}{3}\left(\bar{K}_p + \frac{2\bar{C}_p}{\Delta t}\right) \\ K_2 &= \frac{4}{3}\frac{\bar{C}_s}{\Delta t} \end{aligned}\right\} \tag{10a}$$

and

$$\{\Delta\varepsilon'\} = \frac{4}{3}\left[\frac{\bar{C}_s}{k_2}\{\dot{\varepsilon}^c_{\text{total}} - \dot{\varepsilon}^c_{\text{primary}}\} + \frac{\bar{C}_p}{k_1}\{\dot{\varepsilon}^c_{\text{primary}}\}\right] \tag{14a}$$

The creep strain rates in Eq. (5) may be rewritten likewise, i.e. in terms of deviatoric stresses

$$\{\dot{\varepsilon}^c_{\text{total}}\} = \frac{3}{2\bar{C}_s}\{S\} + \{\dot{\varepsilon}^c_{\text{primary}}\}$$

$$\{\dot{\varepsilon}^c_{\text{primary}}\} = \frac{3}{2\bar{C}_p}\{S\} - \frac{\bar{K}_p}{\bar{C}_p}\{\varepsilon^c_{\text{primary}}\} \tag{5a}$$

Upon substitution of Eq. (5a), the psuedo incremental strain in Eq. (14a) is reduced to

$$\{\Delta\varepsilon'\} = 2\left(\frac{1}{k_1} + \frac{1}{k_2}\right)\{S\} - \frac{4}{3}\frac{R_p}{k_1}\{\varepsilon^c_{primary}\} \quad . \tag{14b}$$

In the absence of plastic deformation, the total strain increment may be expressed as

$$\{\Delta\varepsilon^e + \Delta\varepsilon^c\} = [D_e^{-1} + D_c^{-1}]\ \{\Delta\sigma\} \tag{19}$$

where D_e and D_c are material matrices for elasticity and creep, respectively.

Notice that the total strain increment must be corrected with a pseudo incremental strain vector $\{\Delta\varepsilon'\}$, in Equation (14b), i.e.,

$$\{\Delta\varepsilon^e + \Delta\varepsilon^c\} = \{\Delta\varepsilon - \Delta\varepsilon'\} \tag{20}$$

Combining Equations (19) and (20), we obtain

$$\{\Delta\sigma\} = [D_{ec}]\ \{\Delta\varepsilon - \Delta\varepsilon'\} \tag{21}$$

where

$$[D_{ec}] = [D_e^{-1} + D_c^{-1}]^{-1}.$$

For isotropic material, the elastic-creep tangent matrix $[D_{ec}]$ may be conveniently obtained by

$$[D_{ec}] = \begin{bmatrix} K + \frac{2}{3} k_{ec} & K - \frac{1}{3} k_{ec} & K - \frac{1}{3} k_{ec} & 0 & 0 & 0 \\ & K + \frac{2}{3} k_{ec} & K - \frac{1}{3} k_{ec} & 0 & 0 & 0 \\ & & K + \frac{2}{3} k_{ec} & 0 & 0 & 0 \\ & & & \frac{1}{2} k_{ec} & 0 & 0 \\ & \text{SYM} & & & \frac{1}{2} k_{ec} & 0 \\ & & & & & \frac{1}{2} k_{ec} \end{bmatrix} \quad (22)$$

where the stiffness for the elastic-creep element is obtained from

$$\frac{1}{k_{ec}} = \frac{1}{2G} + \frac{1}{k_c}$$

and a bulk modulus from

$$K = \frac{E}{3(1-2\nu)} \quad .$$

VI. COUPLING OF PLASTICITY AND THE SOLUTION METHOD

When the plastic deformation is involved in the creep analysis, the plastic strain increment should be included in the total strain increment in Eq. (20). The plastic strain increment may be obtained by

$$\{\Delta\epsilon^P\} = D_p^{-1} \{\Delta\sigma\} \tag{23}$$

where

$$D_p^{-1} = \frac{1}{H} \left\{\frac{\partial f}{\partial \sigma}\right\} \left\{\frac{\partial f}{\partial \sigma}\right\}^T$$

with plasticity modulus $H = \frac{d\bar{\sigma}}{d\bar{\epsilon}^p}$ and the function (f) defining effective stress. Introducing Eq. (23) into Eq. (21), the elasto-plastic-creep stress-strain relations are established as

$$[D_e^{-1} + D_c^{-1} + D_p^{-1}] \{\Delta\sigma\} = \{\Delta\epsilon - \Delta\epsilon'\} \tag{24}$$

from which the stress increment vector $\{\Delta\sigma\}$ can be obtained.

The creep deformation tends to relax the stresses in the absence of further increments in external loads. In the creep dominant process, therefore, plastic deformation could only be induced by creep to alleviate stresses in the neighboring material. For this reason, MSC/NASTRAN solves the elasto-plastic-creep problem in two distinct steps using the elastic-creep tangent matrix in Eq. (22).

If there is no plastic deformation during the time interval (Δt), the net stress increment can be computed as in Eq. (21). Then the yield function should be evaluated to check if in fact yielding did not occur during that interval, i.e.

$$F(\sigma) = f(\sigma) - Y(\bar{\epsilon}^P) < 0 \tag{25}$$

with $\sigma = \sigma_{old} + \Delta\sigma$

where $Y(\bar{\varepsilon}^p)$ is the yield stress corresponding to the current plastic state represented by the effective plastic strain $(\bar{\varepsilon}^p)$. If $F(\sigma) < 0$, the solution at this point is valid. But if there was any plastic flow during this time interval, i.e. $F(\sigma) > 0$, Eq. (24) may be rearranged as

$$\{\Delta\sigma\} = [D_{ec}]\ \{\Delta\varepsilon - \Delta\varepsilon'\} - \Delta\lambda[D_{ec}]\ \{\frac{\partial f}{\partial\sigma}\} \tag{26}$$

where

$$\Delta\lambda = \frac{\{\frac{\partial f}{\partial\sigma}\}^T D_{ec}\{\Delta\varepsilon - \Delta\varepsilon'\}}{H + \{\frac{\partial f}{\partial\sigma}\}^T D_{ec}\{\frac{\partial f}{\partial\sigma}\}} \equiv \Delta\bar{\varepsilon}^p > 0 \quad .$$

The algorithm is described by a flow diagram in Figure 4.

VII. RECOVERY OF CREEP STRAINS

The total creep strain increment vector can be recovered by subtracting $\{\Delta\varepsilon^e\}$ and $\{\Delta\varepsilon^p\}$ from $\{\Delta\varepsilon\}$ in Eq. (24) i.e.,

$$\{\Delta\varepsilon^c_{total}\} = [D_c^{-1}]\{\Delta\sigma\} + \{\Delta\varepsilon'\} = \frac{1}{k_c}\{\Delta s\} + \{\Delta\varepsilon'\} \tag{27}$$

where

$$\{\Delta s\}^T = \langle \Delta\sigma_x' \ \Delta\sigma_y' \ \Delta\sigma_z' \ 2\Delta\tau_{xy} \ 2\Delta\tau_{yz} \ 2\Delta\tau_{zx} \rangle \ .$$

The primary creep strain increment vector must be recovered by considering the response of the primary creep element alone, i.e.,

$$\{\Delta\varepsilon^c_{primary}\} = \frac{1}{k_1}\{\Delta s\} + \{\Delta\varepsilon'_{primary}\} \tag{28}$$

where $$\{\Delta\varepsilon'_{primary}\} = \frac{2}{k_1}\{s\} - \frac{4}{3}\frac{K_p}{k_1}\{\varepsilon^c_{primary}\} \ .$$

Then the primary creep strain must be updated as

$$\{\varepsilon^c_{primary}\} = \{\varepsilon^c_{primary}\} + \{\Delta\varepsilon^c_{primary}\} \ . \tag{29}$$

Some of the Equations (16) through (29) are reduced to much simpler forms for uniaxial, plane stress and plane strain cases, which are omitted in the discussion for brevity.

VIII. PROGRAM VERIFICATION

Included in these examples are a part of the problems used to verify the creep capabilities with respect to the algorithm, accuracy and coding errors. Several of these problems examine numerous possible paths by using uniaxial loading on various elements connected in various configurations.

Figure 5 shows verification of various creep laws in the form of Eq. (1) and the direct input of rheological creep parameters. MSC/NASTRAN tracked the curves accurately, showing errors less than 0.1% in the creep strain at the end of 70 steps (t = 800 hours). Figure 6 shows verification of creep laws in the form of Eq. (2). In this case, there exists an error because of mismatch between the empirical formula and the rheological model. The error is accumulated up to 15-19% in the creep strain at the end of 70 steps (t = 6 hours).

The creep analysis capability under variable temperatures is provided by a thermodynamic consideration for the microscopic behavior of the material as expressed in Eq. (3). For verification, empirical creep laws recommended by the Oak Ridge National Laboratory are selected. There are two different creep laws (types 111 and 121 in Figure 7) for the same material (type 304 stainless steel) established at different temperatures (1100° F and 1200° F). The creep law type 111 represents the creep behavior at 1100° F. This creep law is applied at the operating temperature of 1200° F with corrections for the variable temperature. The results are compared with the creep law type 121, which predicts proper creep behavior at 1200° F. As shown in Figure 7, the correction scheme improves the solution, but the accuracy is satisfactory only for a short period of time. Small temperature variations would also help to improve the accuracy. Such a capability, however, is rarely available in the industry and it is an essential feature to analyze creep behavior under varying temperatures.

Coupling of the plastic deformation with creep is verified by reproducing the isochronous stress-strain curve at 100 hours as shown in Figure 8. An isochronous stress-strain curve is a plot of the stress as a function of total strain, which represents a locus of total strains accumulated when various

constant stresses are applied for a fixed time. The data points are obtained in 15 steps to the creep time of 100 hours.

The creep behavior is manifested in the relaxation process under constant strain. Figure 9 compares relaxation predictions by various methods. Superiority of the tangent modulus method over initial strain method is demonstrated.

Figure 10 shows the creep response of various elements under uniaxial tension of 12.5 ksi for 500 hours, 15 ksi for 500 hours and -12.5 ksi for 500 hours. The effects of the creep strain hardening are exhibited properly with a stress reversal. All the elements (rod, shell and solid) produced identical results when a proper time increment (Δt) and the iteration method are used. It is noted that as the stress reverses the direction, the convergence required a stiffness matrix update (SEMI or SEMIQN method) and the smaller time increment. With larger time increments, solutions to the solid model showed a deterioration in accuracy first.

IX. EXAMPLE PROBLEMS

1. Plane Strain Case

The classical creep problem, to which an analytical solution exists, is presented to illustrate a creep analysis capability by MSC/NASTRAN. It is a problem of an infinitely long thick-walled cylinder with inside and outside radii of 0.16 inch and 0.25 inch, respectively, subjected to internal pressure of 35 psi. The assumption of infinite length imposes a plane strain condition. The creep behavior is assumed to obey the simple empirical creep law, which accounts for only secondary creep, i.e.,

$$\varepsilon^c = (6.4 \times 10^{-18})(\sigma^{4.4})t$$

where σ and t are measured in psi and hour, respectively.

By virtue of axisymmetry and a plane strain condition, modeling is simplified by allowing only radial displacement degrees-of-freedom (DOF). A cylindrical coordinate system (CØRD1C card) is employed. Two models are constructed as shown in Figure 11 to verify plane strain element capability.

One of the models consists of nine plane strain elements with 20 active DOFs. The internal pressure of 365 psi is simulated by two FØRCE cards applied to the nodal points on the inside radius. Notice that the plane strain elements (QUAD4) can be attained by specifying -1 in the fifth field of the PSHELL card. The other model is constructued using 9 HEXA elements with axisymmetric and plane strain boundary conditions, consisting of 40 active DOFs. The internal pressure is applied by a PLØAD4 card.

The material is assumed incompressible (using $\nu = 0.499$) with a Young's modulus of 20×10^6 psi. Creep characteristics are defined on the CREEP card which is associated with the MAT1 card by the same ID number in data Field 2 of both cards. The creep analysis requires an initial solution at $t = 0$, which is accomplished by a subcase with $\Delta t = 0$, specified in the DT field of the NLPARM card. Three subsequent subcases are used for creep analysis with various values of Δt, maintaining the constant load. Solutions from the plane strain QUAD4 model do not match solutions from the HEXA model. Stresses are

as much as 20% different from the correct solution, because the plane strain QUAD4 element is not capable of representing incompressibility properly due to its inherent limitations. This point was verified by another computer run for compressible material. Solutions with $\nu = 0.3$ for the plane strain elements match those from the HEXA model within a 0.2% error in stresses. Solutions for the HEXA model with $\nu = 0.499$ are compared with Reference [2] in Figures 12 and 13. The agreement of the results with the Reference is excellent.

2. Axisymmeric Case

The creep behavior of a thick-walled pressure vessel with a flat-end closure (defined in Reference [2]) is analyzed under an internal pressure of 445 psi. The geometry of the pressure vessel is defined as follows:

Overall length	0.89	inch
Outside radius	0.25	inch
Inside radius	0.159	inch
Wall Thickness (uniform)	0.091	inch
Fillet radius	0.03	inch

The material has the following elastic properties:

Young's Modulus	20×10^6 psi
Poisson's Ratio	0.3

and is assumed to obey an empirical creep law in the form of

$$\varepsilon^c = (19.8 \times 10^{-16})(\sigma^{3.61})(t^{1.06})$$

where σ and t are measured in psi and hours, respectively.

The modeling is simplified by axisymmetry and symmetry about the mid-plane. A finite element model as shown in Figure 14 is constructed using 72 solid elements (4 PENTAs and 68 HEXAs) with 355 active DOFs. Appropriate boundary conditions are imposed for symmetry (using SPC1, SPCADD and GRDSET cards) in the cylindrical coordinate system (CØRD1C). A local coordinate system (CØRD2C) is used to specify the geometry of a toroidal section. The internal pressure is applied by PLØAD4 cards. Although the applied load does not produce plastic deformation, all the elements are treated as being made of elasto-plastic-creep material by attaching MATS1 and CREEP cards to the MAT1

card.

The internal pressure of 445 psi is applied in the first subcase for the initial static solution. Creep analyses are performed in the subsequent subcases by applying a nonzero time increment while the applied pressure is kept constant. Six subcases (only two subcases are activated on the listing shown in Table 1) are set up as follows:

Subcase ID	KMETHØD	INCREMENTS	Δt (Hour)	Ending Creep Time (Hour)*
100	AUTØ	1	0.	0.
200	SEMIQN	5	0.02	0.01
300	AUTØQN	9	0.1	1.0
400	AUTØQN	10	0.1	2.0
500	AUTØQN	5	0.2	3.0
600	AUTØQN	5	0.4	5.0

* Notice that the creep time interval is gradually increased.

The computer run was stopped after every subcase to obtain the stress contour plot. Then the analysis was continued by restarting from the last converged solution. The entire analysis took six runs (five restarts) to obtain solutions up to five hours of creep. Each creep solution took three to four iterations to converge (average 10 CPU minutes on the VAX 11/780).

Figures 15 and 16 show stress contours at t = 0 and 3, respectively. The stress history at two selected points (junction of the cylinder and end closure) are shown in Figure 17. It can be seen that the steady-state stress is reached after approximately three hours of creep. Notice that MSC/NASTRAN shows a higher stress level at the inside surface (where the stress concentration occurs) throughout the analysis. Since the initial stress is similarly higher, this error is actually a consequence of a coarse mesh. Also, notice that the point with higher stress relaxes a little faster than might be expected. More accurate solutions should be obtained with a finer mesh around the fillet area.

X. CONCLUDING REMARKS

The creep analysis capability of MSC/NASTRAN is a generalization of the viscoelastic material capability. The validity of the theory and the algorithm are proven and the analysis results show close agreement with experiment and other analysis methods. This capability can be extended for further generalization of the viscoelastic capability by coupling creep with nonlinear elastic material capability.

References

1. M. P. Badani, "A New Method to Solve Nonlinear Creep Problems in Structural Mechanics Using Incompatible Isoparametric Finite Elements," Ph.D. Dissertation, U. C. Berkeley, 1980.

2. G. A. Greenbaum and M. F. Rubinstein, "Creep Analysis of Axisymmetric Bodies Using Finite Elements," Nuclear Engineering and Design, Vol. 7, 1968.

3. O. C. Zienkiewicz, "The Finite Element Method," McGraw-Hill, 1977.

4. H. Kraus, "Creep Analysis," John Wiley and Sons, 1980.

5. N. H. Polakowski and E. J. Ripling, "Strength and Structure of Engineering Materials," Prentice-Hall, 1966.

6. R. C. Juvinall, "Stress, Strain and Strength,: McGraw-Hill, 1967.

7. J. A. Clinard, et. al., "Elevated-Temperature Deformation and Failure Testing and Analysis of Nozzle-to-Spherical Shells: Specimens NS-2 and NS-1," Oak Ridge National Laboratory, ORNL-5939, January 1983.

8. A. Levy and A. B. Pifko, "On Computational Strategies for Problems Involving Plasticity and Creep," International Journal for Numerical Methods in Engineering, Vol. 17, 1981.

9. Sang H. Lee, "Design Document for Creep Analysis Capability," The MacNeal-Schwendler Corporation, SHL-8, June 2, 1982.

10. Sang H. Lee, "Organization of the Elasto-plastic Material Routine," The MacNeal-Schwendler Corporation, SHL-9, April 29, 1982.

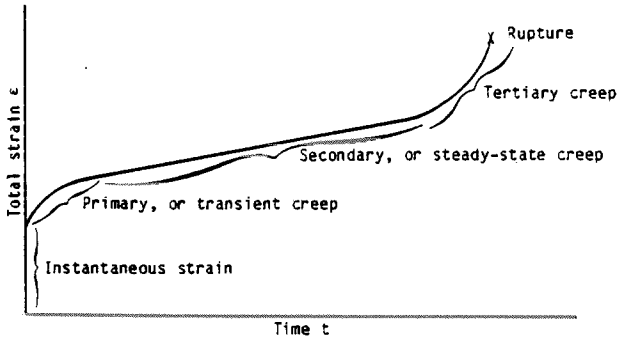

Figure 1. Uniaxial Creep Test Under Constant Load at Constant Temperature

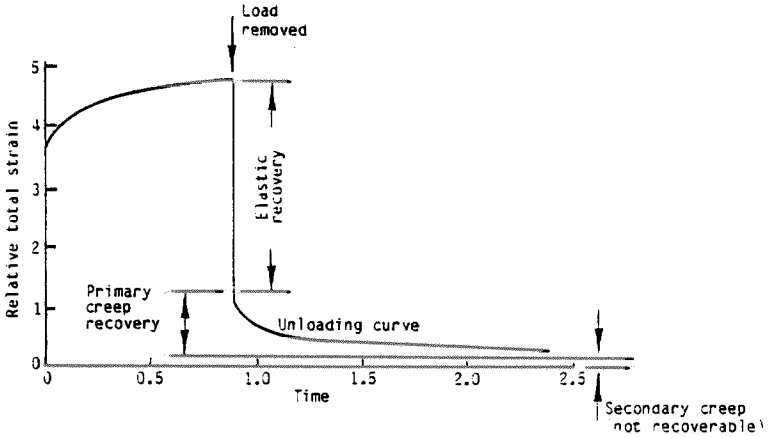

Figure 2. Creep Strain Relaxation Upon Load Removal

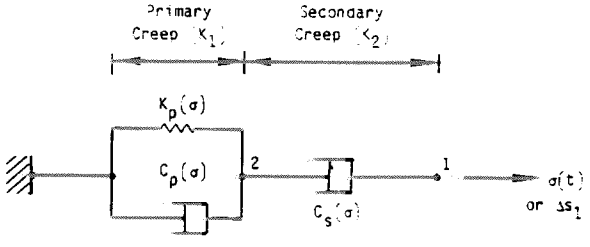

Figure 3. Rheological Model.

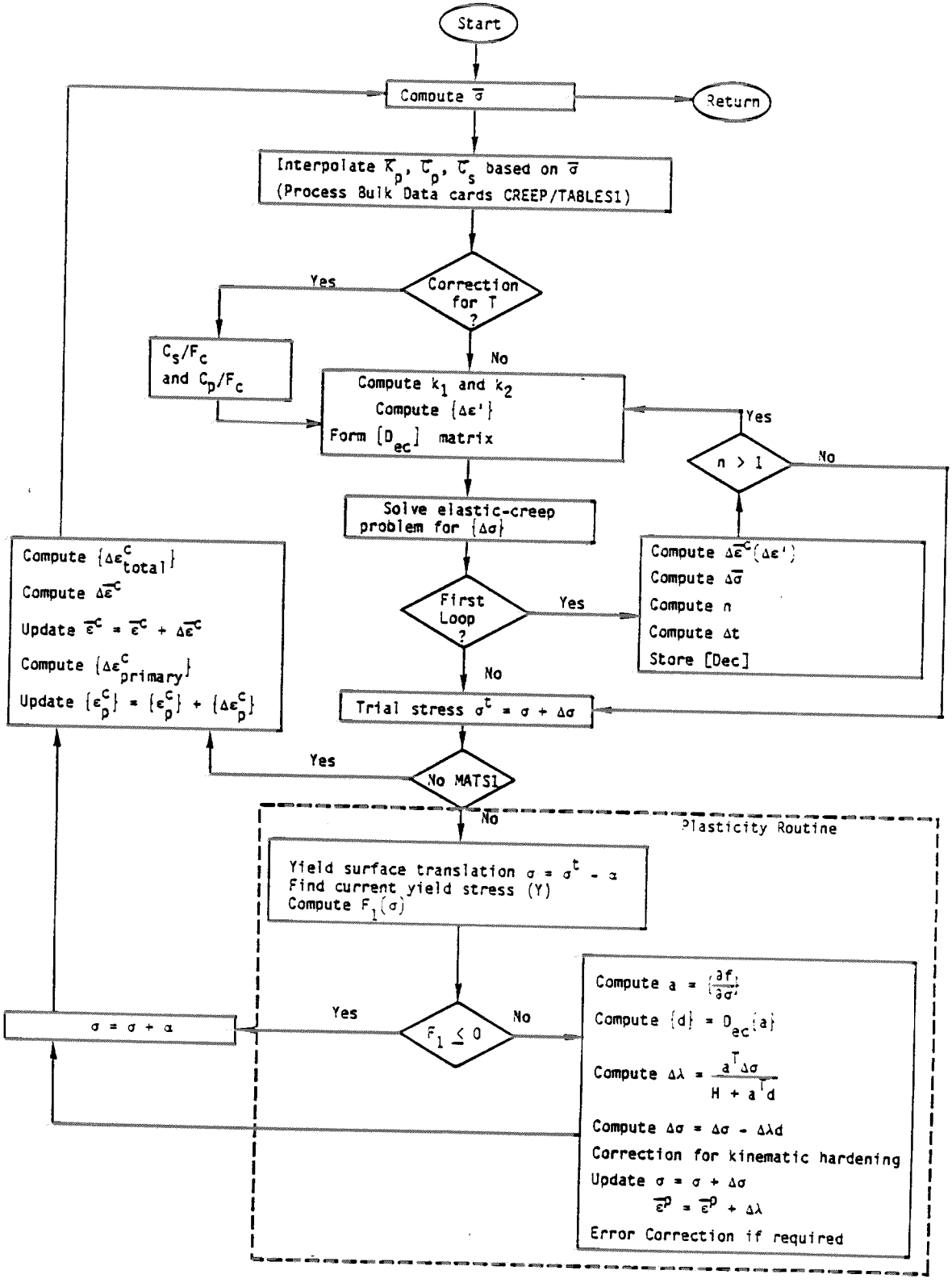

Figure 4. Flow Diagram for Creep Material.

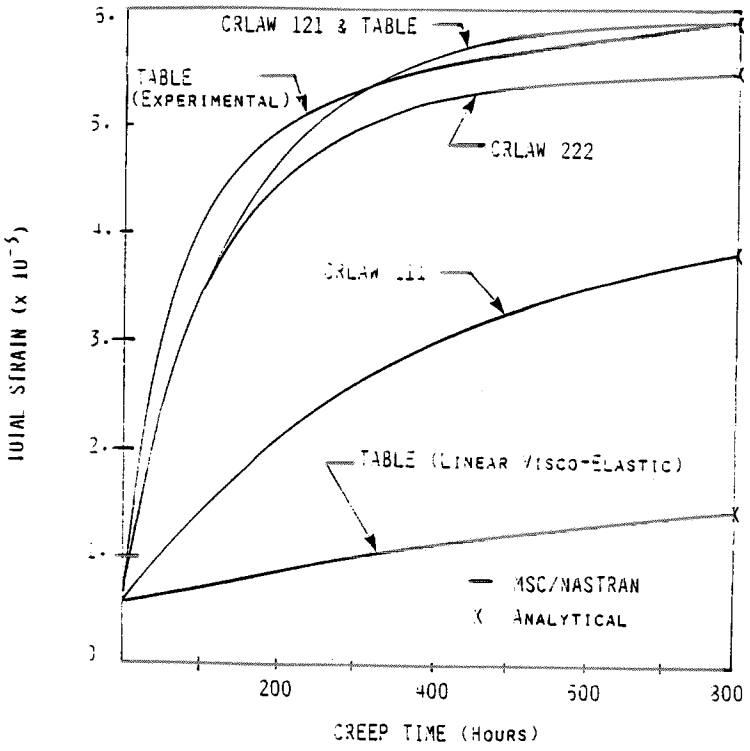

Figure 5. Verification of Creep Laws in Equation (2) and TABLE Inputs.

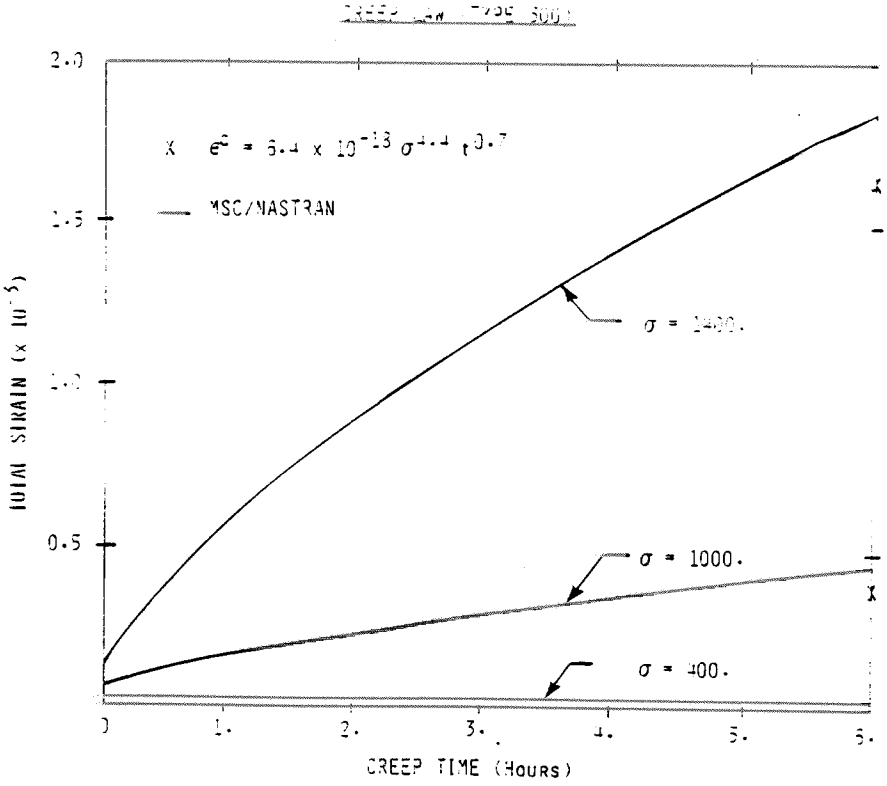

Figure 6. Verification of Creep Laws in Equation (3).

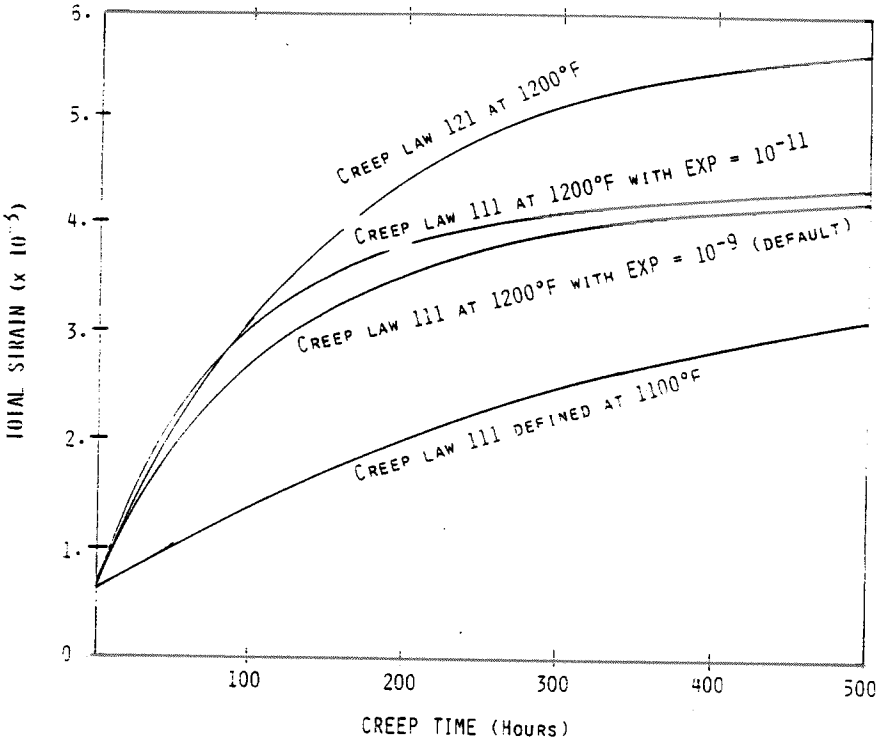

Figure 7. Creep Capability Verification for Variable Temperature Problem.

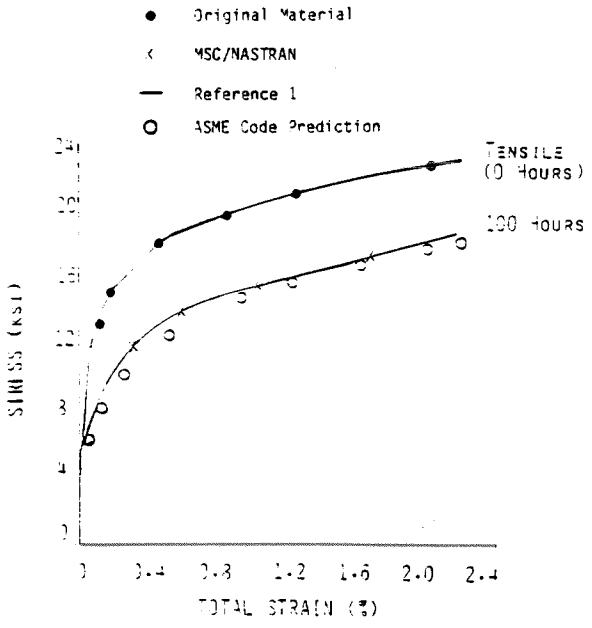

Figure 8. Verification of Elasto-plastic Creep Analysis by Isochronous Stress-strain Curve.

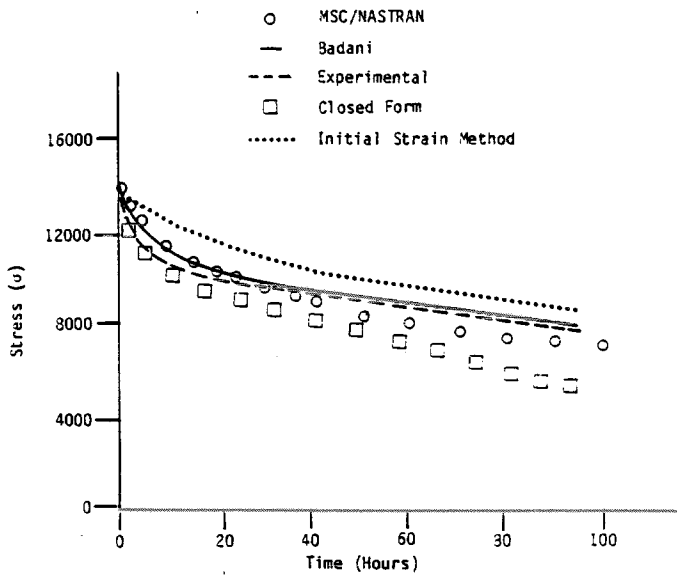

Figure 9. Comparison of Creep Relaxation Predictions.

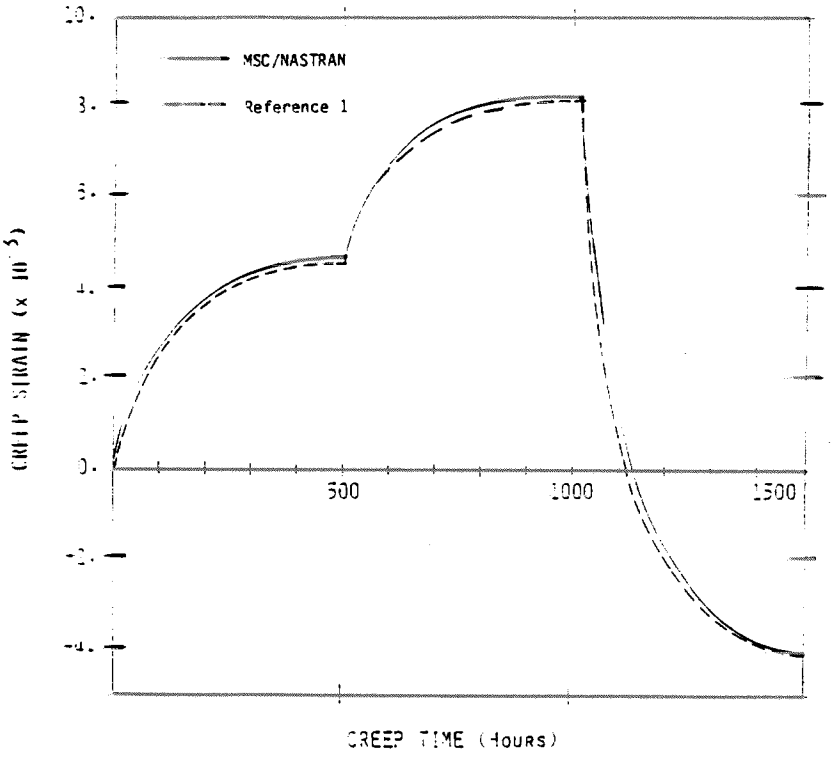

Figure 10. Effects of Creep Strain Hardening Demonstrated Under the Step Loading with Stress Reversal.

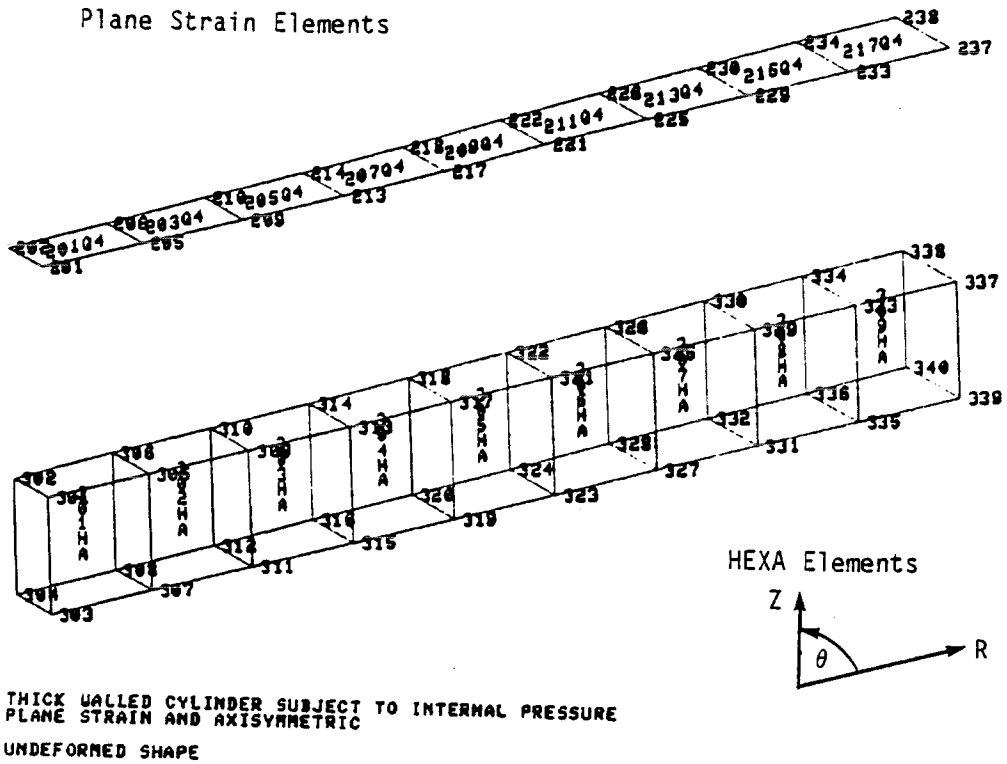

Figure 11. Isometric View of MSC/NASTRAN Model.

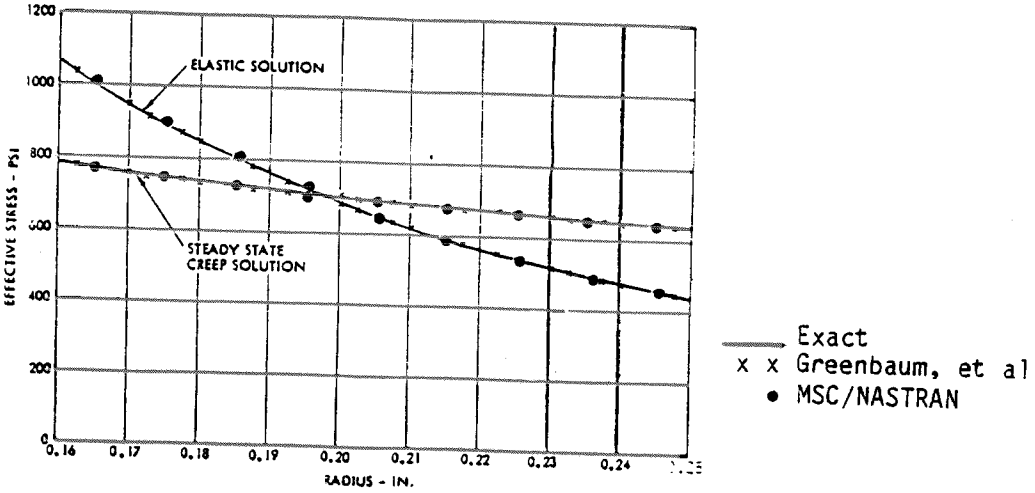

Figure 12. Effective Stress Distribution in a Thick-Walled Cylinder.

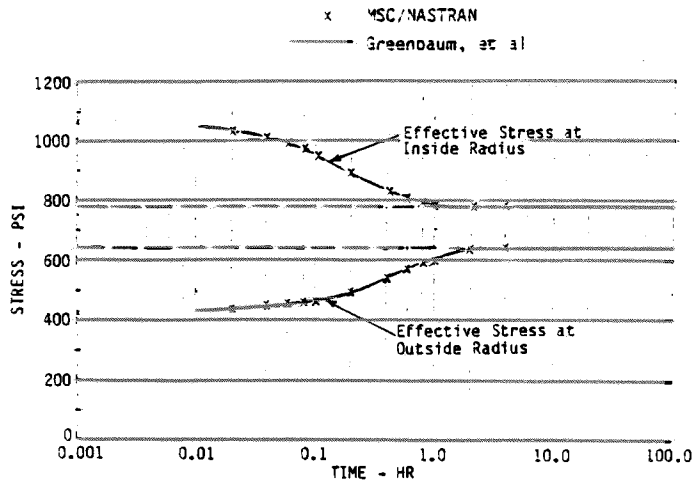

Figure 13. Stress Relaxation for a Thick-Walled Cylinder.

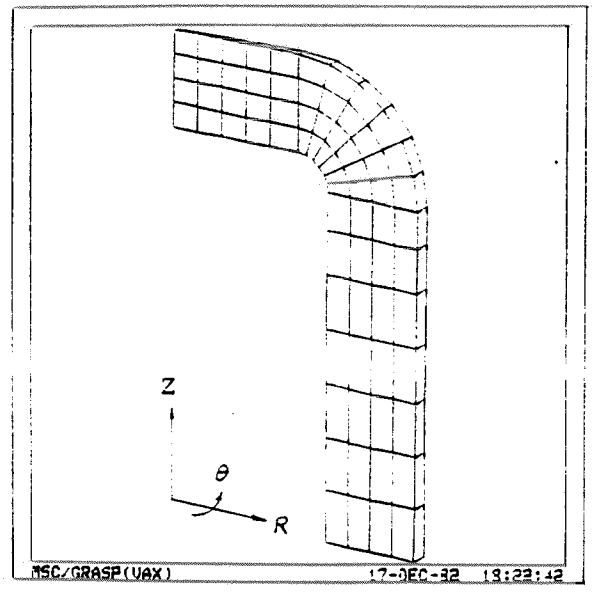

Figure 14. Finite Element Model of Pressure Vessel.

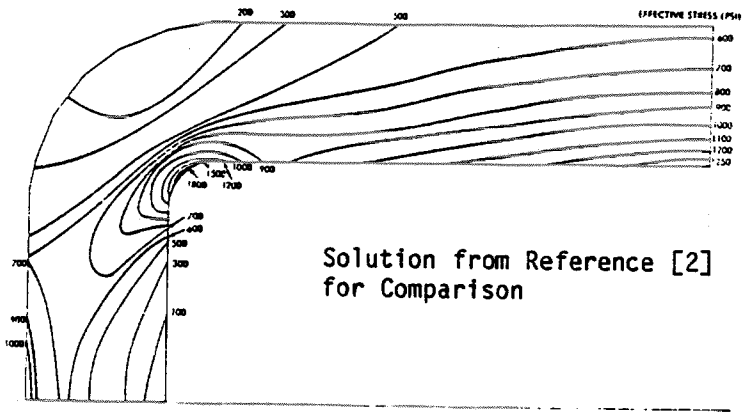

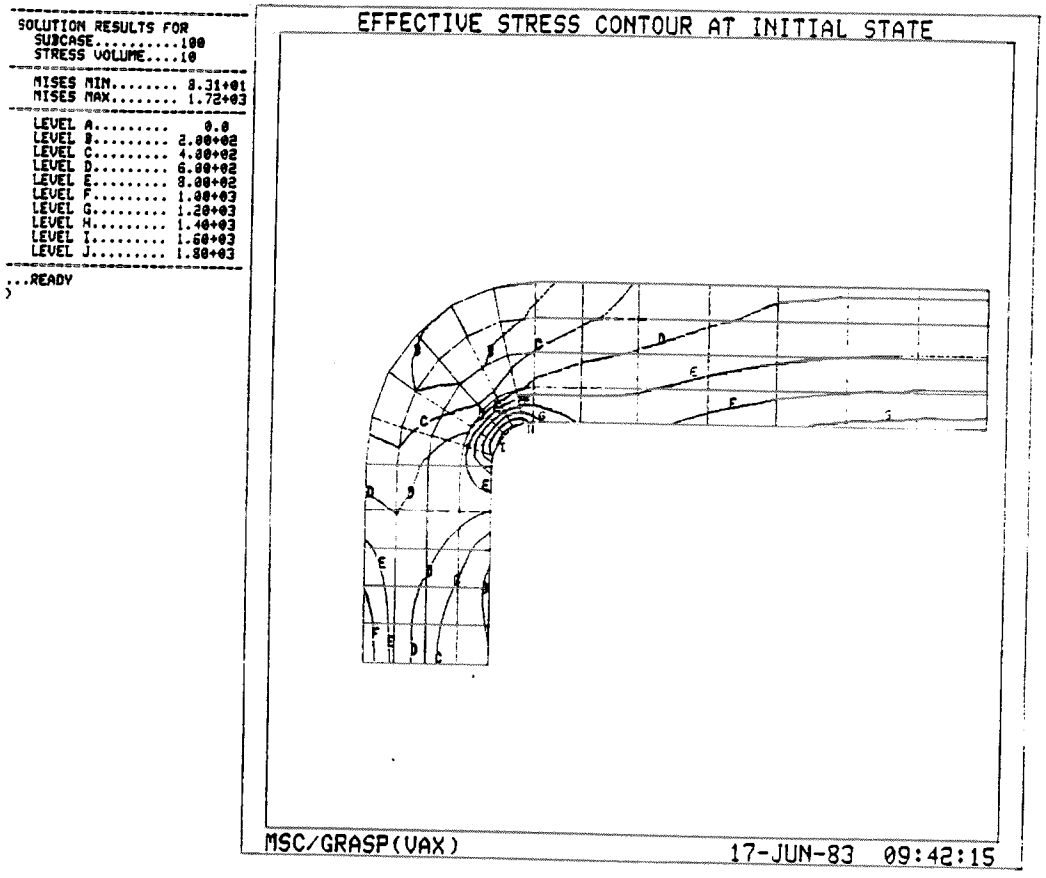

Figure 15. Initial Stress Distribution (Effective Stress).

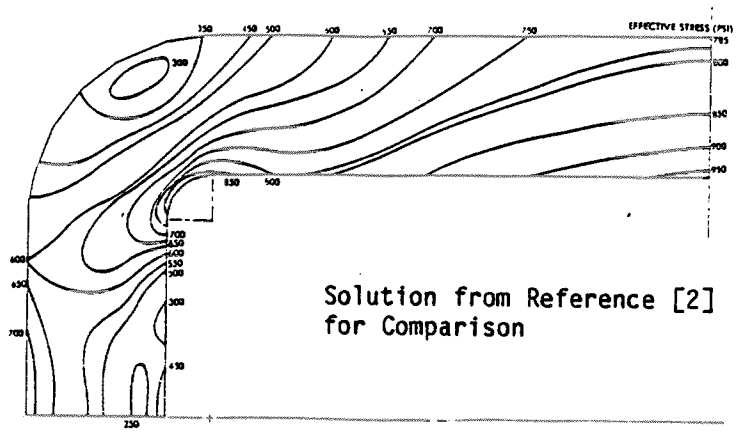


```
 SOLUTION RESULTS FOR
    SUBCASE.....500
    STRESS VOLUME....10

    MISES MIN..... 2.29+02
    MISES MAX..... 9.64+02

    LEVEL B..... 2.00+02
    LEVEL C..... 3.00+02
    LEVEL D..... 4.00+02
    LEVEL E..... 5.00+02
    LEVEL F..... 6.00+02
    LEVEL G..... 7.00+02
    LEVEL H..... 8.00+02
    LEVEL I..... 9.00+02
    LEVEL J..... 1.00+03

...READY
>
```

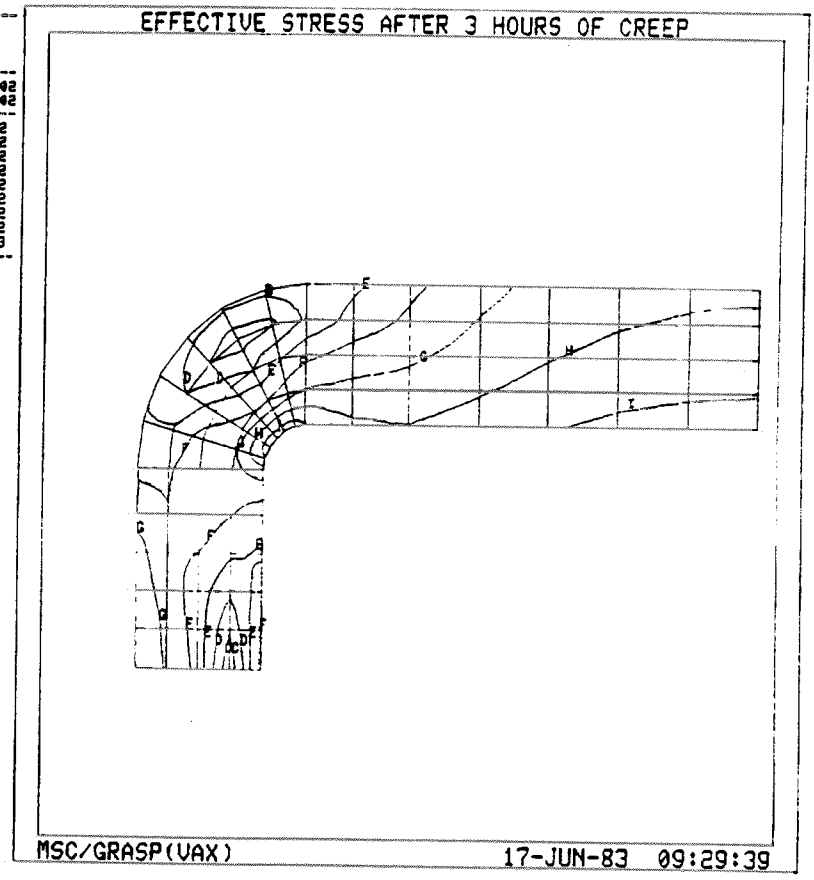

Figure 16. Stress Distribution at t = 3 Hours (Effective Stress).

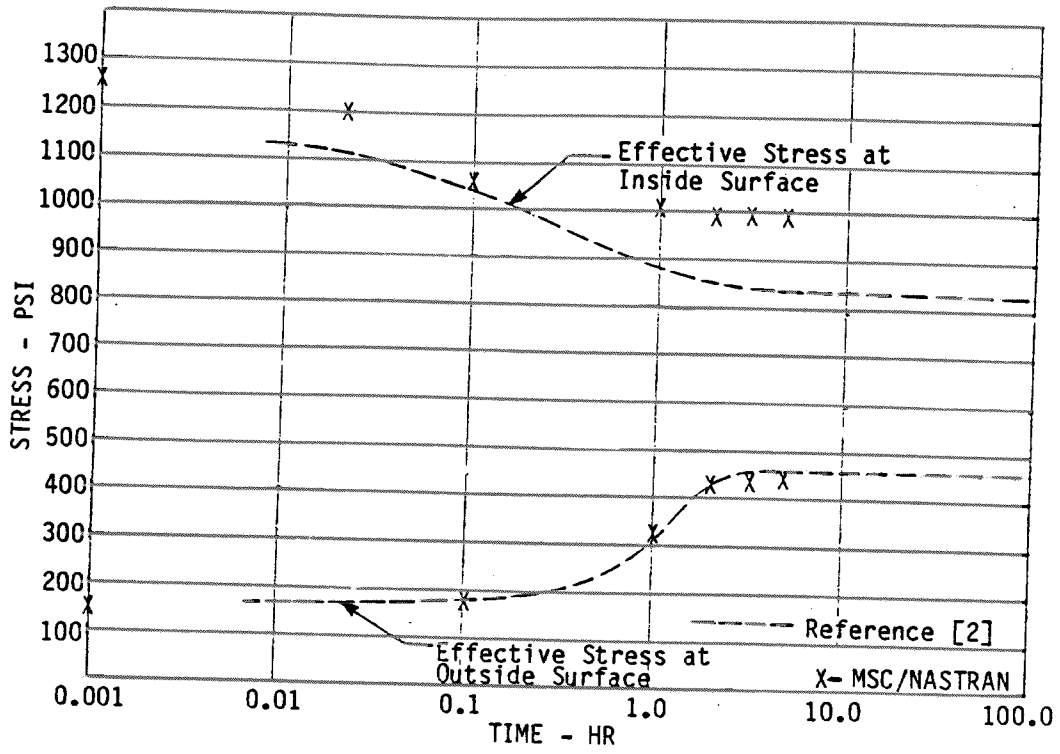

Figure 17. Stress Relaxation at the Junction of the Cylinder and End Closure.